System Identification Modeling of a Model-Scale Helicopter

Bernard Mettler and Takeo Kanade
The Robotics Institute
Carnegie Mellon University
Pittsburgh, Pennsylvania

Mark B. Tischler
Army/NASA Rotorcraft Division
Aeroflightdynamics Directorate
Ames Research Center

CMU-RI-TR-00-03

Abstract: Development of a reliable high-performance helicopter-based unmanned aerial vehicle (UAV) requires an accurate and practical model of the vehicle dynamics. This report describes the process and results of the dynamic modeling of a model-scale unmanned helicopter (Yamaha R-50 with 10 ft rotor diameter) using system identification. A complete dynamic model was derived for both hover and cruise flight conditions. In addition to standard helicopter flight characteristics, the model explicitly accounts for the stabilizer bar, which has a strong influence on the flight dynamics and is widely used in model-scale helicopters. The accuracy of the developed model is verified by the comparison between predicted and actual responses from the model and the flight experiments (in both frequency and time domains), and between key identified parameters and their theoretical values. Scaling of the main characteristics of the R-50 model-scale helicopter with respect to those of a UH-1H full-size helicopter was performed to determine how the size influences the flight dynamics of helicopters.

1 Introduction

Model-scale helicopters are increasingly popular platforms for unmanned aerial vehicles (UAVs). The ability of helicopters to take off and land vertically, to perform hover flight as well as cruise flight, and their agility and controllability, make them ideal vehicles for a range of applications which can take place in a variety of environments. Existing model-scale helicopter-based UAVs (HUAVs), however, exploit only a modest part of the helicopter's inherent qualities. For example, their operation is generally limited to hover and slow-speed flight, and their control performance is in most cases sluggish. These limitations on HUAV operation are mainly the consequence of a poor flight control system.

Throughout the 1990's, most HUAVs used classical control systems such as single-loop PD systems. The controller parameters are usually tuned manually for a distinct operating point (generally hover flight). This situation is surprising given the abundance of effective multivariable controller synthesis methods. One reason for this situation is that most multivariable control methods are model-based, and that dynamic models for a particular model-scale helicopter are not readily available.

The dynamic models used for controller synthesis or controller optimization have strict requirements. The model must capture the effects that govern the performance and maneuverability of the vehicle. High-bandwidth control requires models with high-bandwidth accuracy. For helicopters, this implies that they must explicitly account for effects such as the rotor/fuselage coupling. At the same time the model must be simple enough to be insightful and practical for the control synthesis.

Using a standard first-principle based modeling approach, considerable knowledge about rotorcraft flight dynamics is required to obtain the governing equations, and comprehensive flight validations and model refinements are necessary before sufficient accuracy is attained. Instead, in the helicopter community a modeling method based on system identification has been developed and successfully used with full-scale helicopters. The experimental nature of a system-identification based method enables the engineer to recognize the key flight-dynamic characteristics of the vehicle, and thus allows the engineer to concentrate the modeling effort on these characteristics.

Only a few examples of the application of system identification techniques to the modeling of model-scale helicopters exist. The results obtained are limited compared with what is regularly achieved with full-scale helicopters. For example, a low-order model (rigid body dynamics) was identified using experiments with a rigged helicopter [1], or only the longitudinal stability and control derivatives were identified [2].

This report describes the first comprehensive application of system identification techniques to a model-scale helicopter. Both hover and cruise flight conditions have been treated and all the effects which are important for the performance and maneuverability of a model-scale helicopter have been captured. The experiments were conducted on Carnegie Mellon's HUAV, which is based on a Yamaha R-50 model scale helicopter. For the identification, a frequency-domain method developed by the US Army and NASA was used (Comprehensive Identification from FrEquency Responses CIFER® [3]).

Figure 1 - Instrumented R-50 in hovering flight

The report is organized as follows: In Section 2, we describe the principal physical and flight-mechanical characteristics of the R-50 model-scale helicopter, as well as the instrumentation and on-board systems. In Section 3, we present the fundamentals of the CIFER® identification method. Section 4 describes the flight-testing performed for the collection of the flight-data. In Section 5, we explain the identification process, concentrating on the definition of the state-space model structure used in the identification. In Section 6, we present the identification results: first, the agreement between the predicted frequency responses from the identified model and the actual frequency responses from the flight-data; second the identified model parameters, along with, when possible, a comparison of their values wtih the values predicted by helicopter theory; and finally, the agreement between the predicted and actual time responses. Then, we present analytical results: first the eigenvalues and dynamic modes, and second a comparison between characteristic parameters of the model-scale helicopter and those of a full-scale helicopter scaled to the same rotor diameter.

2 Description of the CMU Helicopter

2.1 Yamaha R-50 Helicopter

The Yamaha R-50 helicopter used in the HUAV project at Carnegie Mellon University (CMU) (Figure 1) is a commercially available model-scale helicopter originally designed for remote operated crop-dusting. Because of the adequate payload (20 kg) and the general ease of operation, it has become a platform of choice for research in autonomous flight. General physical characteristics of the R-50 are given in Table 1.

The R-50 uses a two-bladed main rotor with a Bell-Hiller stabilizer bar. The relatively rigid blades are connected to a yoke through individual flapping hinges and elastomeric fittings. The yoke itself is attached to the rotor shaft over a teetering hinge in an under-swung configuration, reducing the Coriolis forces and the associated in-plane blade motion. The teetering motion is also restrained by an elastomer damper/spring. This rotor system differs from classical teetering rotors in that it is stiffer and combines teetered and separately hinged blade motion.

The Bell-Hiller stabilizer bar is a secondary rotor consisting of a pair of paddles connected to the rotor shaft through an unrestrained teetering hinge. It receives the same cyclic control input as the main rotor but, due to its different design, it has a slower response than the main blades and is also less sensitive to airspeed and wind gusts. The stabilizer bar flapping motion is used to generate a control augmentation to the main rotor cyclic input. This augmentation is implemented by the bell mixing mechanism. From a control theoretical point of view, the control augmentation can be interpreted as a lagged rate (or “pseudo-attitude”) feedback in the

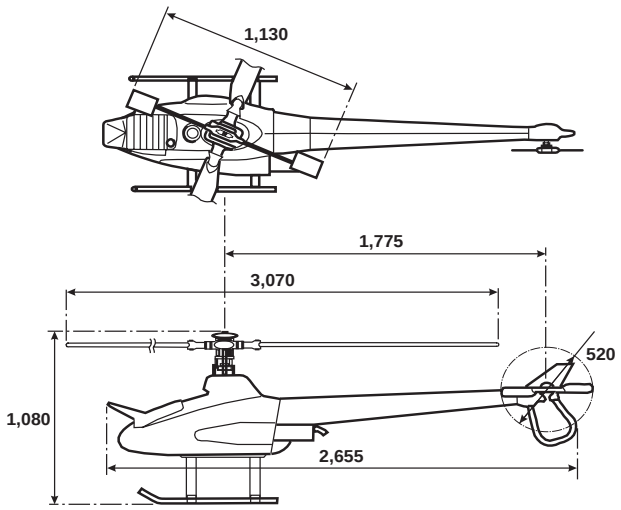

Dimensions	see Figure (units: mm)
Rotor speed Tip speed	850 rpm 449 ft/s
Dry weight Instrumented (full payload capacity)	97 lb 150 lb
Engine type	Single cylinder, 2-stroke, water cooled
Flight autonomy	30 minutes

Table 1 – R-50 Physical Characteristics

pitch and roll loops [4]. The low frequency dynamics are stabilized, which substantially increases the phase margin for pilot/vehicle system in the crossover frequency range ($1-3$rad/s) [4]. The pseudo-attitude feedback also reduces the response of the aircraft to wind gusts and turbulence.

2.2 Scaling Considerations

Stabilizer bars are common in model-scale helicopters because scaling down the helicopter size increases the sensitivity of the dynamics to control inputs and disturbances, and reduces the damping provided by the rotor on the angular pitch and roll motions. Rotor-induced damping arises from the tendency of the rotor disc — therefore of the thrust vector — to lag behind the shaft during pitching or rolling motions. This lag produces a moment about the helicopter's center of gravity opposite to the rolling or pitching direction and proportional to the rolling or pitching rate. A smaller rotor has a smaller rotor time constant τ; therefore, for a given pitch or roll rate, it will lag less and thus produce less damping.

The R-50 is about 1/5-th the size of an average-size manned helicopter (a scale factor N=5 refers to a rotorcraft of 1/5-th the rotor diameter). The rotor time constant τ is a function of the non-dimensional blade lock number γ and the rotor speed Ω ($\tau = 16/\gamma\Omega$). A small rotorcraft has a rotor speed which is about $\sqrt{N}$ faster than the full-size counterpart in order to achieve the same blade tip speed. This means that a small rotorcraft has a $\sqrt{N}$ times smaller rotor time constant and thus a $\sqrt{N}$ smaller rotor induced damping than does its full-size counterpart. A smaller time constant also means a larger bandwidth.

Since the stabilizer bar is not used to produce lift, its dynamic characteristics can be adjusted almost arbitrarily. This property is used in Radio Controlled (RC) helicopters to adjust the flight-dynamic characteristics of the model helicopter to the skills of the pilot.

2.3 HUAV Instrumentation

Carnegie Mellon's HUAV has a state-of-the-art instrumentation capable of producing high quality flight data. The centerpiece of the helicopter onboard systems is a VME-based on-board flight computer which hosts a Motorola 68060 processor board and a sensor I/O board. All sensors and actuators of the helicopter connect through the I/O board with the exception of the inertial measurement unit (IMU), which connects directly to the processor board

through a special serial port. The communication to the ground station takes place via wireless Ethernet. This system runs under a VxWorks real-time operating system.

Three linear servo-actuators are used to control the swash-plate, while another actuator is used to control the pitch of the tail rotor. The dynamics of all the actuators have been identified separately. The engine speed is controlled by a governor which maintains the rotor speed constant in the face of changing rotor load.

The HUAV uses three navigation sensors:

- a fiber-optic based inertial measurement unit (IMU), which provides measurements of the airframe accelerations a_x, a_y, a_z, and angular rates p, q, r (resolution: $0.002\,\mathrm{g}$ and $0.0027°$, data rate: $400\,\mathrm{Hz}$)
- a dual frequency differential global positioning system (GPS) (precision: $2\,\mathrm{cm}$, update rate: $4\,\mathrm{Hz}$)
- a magnetic compass for heading information (resolution: $0.5°$, update rate: $2\,\mathrm{Hz}$)

The IMU is mounted on the side of the aircraft, and the GPS and compass are mounted on the tail. Velocity and acceleration measurements are corrected for the position offset between the helicopter center of gravity and the GPS, or IMU. A 12-th order Kalman filter running at 100 Hz is used to integrate the measurements from the IMU, GPS and compass to produce accurate estimates of helicopter position, velocity and attitude.

3 Frequency-Domain Identification

Frequency responses fully describe the linear dynamics of a system. When the system has nonlinear dynamics (to some extent all real physical systems do), system identification determines the describing functions which are the best linear fit of the system response based on a first harmonic approximation of the complete Fourier series. For the identification, we used a frequency domain method, developed by the U.S. Army and NASA, known as CIFER® (Comprehensive Identification from Frequency Responses) [3]. While CIFER® was developed specifically for rotorcraft applications, it has been successfully used in a wide range of fixed wing and rotary wing, and unconventional aircraft applications [5]. CIFER® provides a set of utilities to support the various steps of the identification process. All the tools are integrated around a database system which conveniently organizes the large quantity of data generated throughout the identification process.

The steps involved in the identification process are:

1. *Collection of flight data*. The flight-data is collected during special flight experiments using frequency sweeps.
2. *Frequency response calculation*. The frequency response for each input-output pair is computed using a Chirp-Z transform. At the same time, the coherence function for each frequency response is calculated.
3. *Multivariable frequency domain analysis*. The single-input single-output frequency responses are conditioned by removing the effects from the secondary inputs. The partial coherence measures are computed.
4. *Window Combination*. The accuracy of the low and high frequency ends of the frequency responses is improved through optimal combination of frequency responses generated using different window lengths.

5. *State-space identification*. The parameters (derivatives) of an a priori-defined state-space model are identified by solving an optimization problem driven by frequency response matching.
6. *Time Domain Verification*. The final verification of the model accuracy is performed by comparing the time responses predicted by the model with the actual helicopter responses collected from flight experiments using doublet control inputs.

4 Flight Testing: Collection of Flight-Data

High quality flight data is essential to a successful identification. The principal concerns are the accuracy of the state estimates (i.e., unbiased, disturbance free, no drop outs), the information content of the flight data (i.e., whether the measurements contain evidence of all the relevant flight-dynamic effects), and the compatibility of the flight data with the postulate of linear dynamics used for the modeling. While the accuracy of the state estimates depends on the instrumentation, the information content and compatibility depends on the execution of the flight experiments.

The responses of the system to low frequency excitations are important for the identification of the speed derivatives ($0.1-1$rad/sec) and the responses to high frequency excitations are important for the identification of the coupled rotor/fuselage dynamics ($8-14$rad/s). To guarantee that the flight data captures the dominant flight-dynamic effects, a frequency-sweep technique is used for the flight testing [6].

By adjusting the magnitude of the excitation, we make sure that the system response remains within a region where the dynamics are predominantly linear. Also, it is important to select a calm day to avoid unmeasured inputs.

A key metric to verify that the flight data is satisfactory for the purpose of system identification is its coherence. The coherence γ_{xy} (or partial coherence for a multiple-input multiple-output system) indicates how well the output y (any of the estimated helicopter state) is linearly correlated with a particular input x over the examined frequency range. It is computed together with the system's frequency responses, from the cross spectrum G_{xy}, and the input and output auto-spectrum G_{xx} and G_{yy} respectively (the partial coherence is derived from the conditioned spectrum).

$$\gamma_{xy}^2 = \frac{|G_{xy}|^2}{G_{xx}G_{yy}} \leq 1 \qquad (1)$$

A coherence larger than 0.6 is considered good. A poor coherence can be attributed to a poor signal-to-noise ratio, nonlinear effects in the dynamics, or the presence of unmeasured inputs such as wind gusts. The coherence is also used as a weighting function in the frequency domain cost function used during the identification of the model parameters.

4.1 Flight-Test Procedure

Two series of flight experiments were organized for each the hover-flight and cruise-flight operating point. For each flight in a series, the pilot applies a frequency sweep control sequence to one of the four control inputs via the remote control (RC) unit. While doing so he uses the other control inputs to hold the helicopter at the selected operating point. In order to gather enough data, the same experiment is repeated several times.

The experiments are conducted open-loop, except for an active yaw damping system, and the stabilizer bar which can be regarded as a dynamic augmentation. An input cross-feed is used

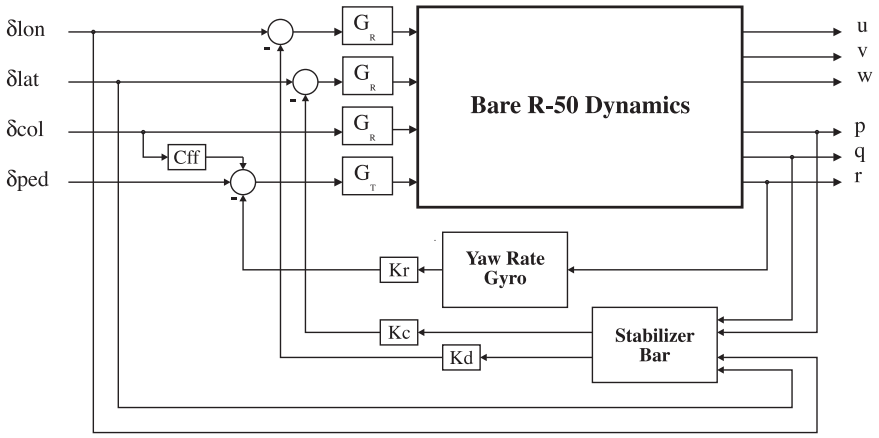

Figure 2 – Augmented R-50 dynamics

by Yamaha between the collective input and the pedal input to compensate for coupling effects between the heave and yaw dynamics.

A block-diagram representing the augmented R-50 dynamics is shown in Figure 2. The inputs to the system are the four helicopter control inputs (cyclic longitudinal δ_{lon} and lateral δ_{lat}, cyclic collective δ_{col} and pedal δ_{ped}) which enter the system via four actuators (three swashplate actuators G_S and one tail actuator G_T). Both the yaw damping system and the stabilizer bar are represented as dynamics augmentations. Only 6 rigid-body fuselage states are illustrated (the three linear velocities u, v, w and the three angular velocities p, q, r).

During the time of the experiment, all control inputs (stick inputs) and all helicopter states are recorded (100Hz sampling rate). Flight-data from the best runs are then concatenated and filtered (-3dB @ 10Hz) to remove undesired information such as structural vibrations. A sample of hover condition flight-data of the longitudinal and lateral response for two concatenated lateral frequency sweeps is shown in Figure 3.

The flight experiments for the hover condition are unproblematic; the helicopter is in the proximity of the pilot and it is relatively easy to hold the operating point.

The cruise-flight experiments are more problematic. We used a fly-over technique: the pilot accelerates the R-50 for a constant distance until the helicopter is directly overhead. At that point, the pilot starts performing the different piloted sweeps while flying down the airstrip and trying to maintain a constant airspeed. We encountered two problems during the cruise-flight experiments. First, it was difficult for the pilot to maintain a precise airspeed because he relied only on the visual sighting for helicopter attitude information. Second, the length of the flight experiment was limited because the helicopter had to be kept in sight.

The record length is critical because it defines the low frequency content of the flight-data ($\omega_{\min} = 2\pi/t_{rec}$). Low frequency information ($0.1-1$rad/sec) is important for the identification of quasi-steady derivatives, such as the speed derivatives. With our experimental method, trying to push the record length degraded the stability of the airspeed. With this tradeoff, by allowing the airspeeds to vary between 10 and 20m/s we were able to achieve a maximum record length of 10s. These issues could be addressed in future experiments by conducting the flight testing on a paved runway and using an automobile as a chase vehicle, or even by performing closed-loop computer-controlled flight testing.

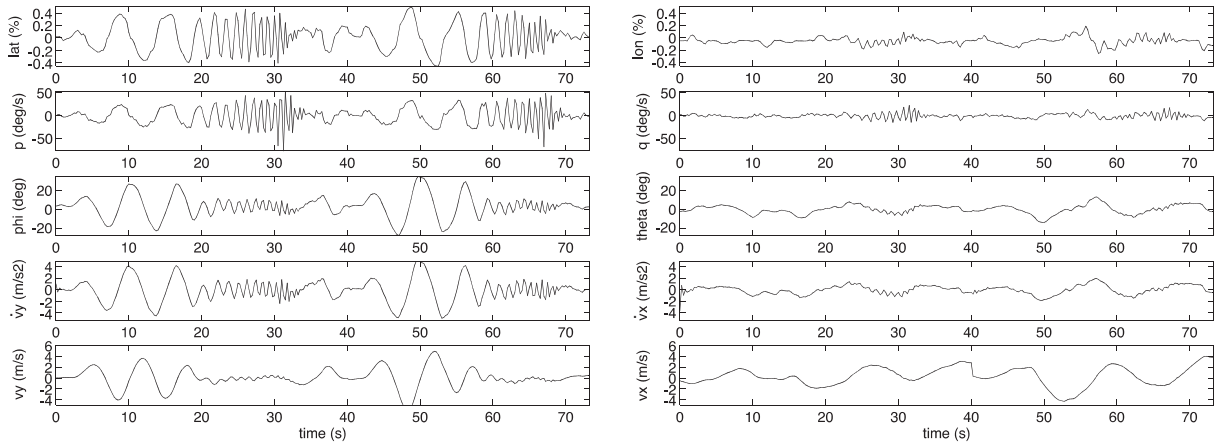

Figure 3 – Sample flight data for two concatenated lateral frequency sweeps

4.2 Flight-Test Results

The frequency responses derived from the hover-flight data and the respective coherence metrics are depicted in Appendix 2a. All on-axis responses attain a coherence close to unity over most of the critical frequency range where the relevant dynamical effects take place. For example, the two on-axis angular rate responses to their respective cyclic inputs achieve a good coherence (≥ 0.6) up to the frequencies of 8–16rad/s, where the important airframe/rotor coupling takes place.

The frequency responses derived from the cruise-flight data and the respective coherence metrics are depicted in Appendix 2b. Here again, all the on-axis responses achieve high coherence values. The generally high coherence obtained for the key helicopter responses speaks for the quality of the helicopter instrumentation, the successfully performed flight experiments, and the dominantly linear behavior of the helicopter around the tested operating conditions.

5 Application of System Identification

Using system identification, we want to achieve the best possible fit of the flight-data with a model that is consistent with the physical knowledge and intuition. The first part of the problem consists of the derivation of the dynamic equations that will define the state-space model with the unknown parameters. Once this is accomplished, the parameters of the model can be identified. Based on the results obtained, the model structure will be refined until satisfactory results are achieved. The criteria used for this iteration are: (i) level of frequency response agreement (frequency error costs), (ii) statistical metrics from the model parameters (insensitivity and Cramer Rao percent), (iv) level of agreement of the system's time responses (time domain verification), and (v) when a specific model parameter has a physical meaning, the level of agreement of the parameter with its theoretical value.

5.1 Building the State-Space Model Structure

The basic equations of motion for a linear model of the helicopter dynamics are derived from the Newton-Euler equations for a rigid body that is free to simultaneously rotate and translate in all six degrees of freedom. The external aerodynamic and gravitational forces are represented by using a stability derivative form. In the simplest model, no additional states are

used, and the control forces produced by the main rotor and tail rotor are expressed by the multiplication of a control derivative and the corresponding control input.

However, a key aspect of helicopter dynamics is the dynamical coupling between the main rotor (which produces most of the control forces and moments) and the helicopter fuselage. Omitting this coupling effect has been shown to limit the accuracy of the helicopter model in the medium to high frequency range [7]. Therefore, for high-bandwidth control design or for handling quality evaluations, it is essential to account for the dynamic coupling between the rotor and the fuselage.

To include the rotor/fuselage coupling the rotor dynamics need to be modeled explicitly and then coupled to the fuselage equation of motions. A standard way to achieve this is the hybrid-model formulation [6] developed originally for full-scale helicopter modeling. Besides the rotor, other effects involving additional dynamics sometimes need to be accounted for. Examples are: the actuators; the engine/drive train system; and control augmentations (such as the active yaw damping system or the stabilizer bar). A more refined model structure has another benefit besides accuracy; the model is physically more consistent, i.e., the model parameters are less lumped and thus physically more meaningful. Our goal was to explicitly model the helicopter dynamics by breaking the system down according to the block-diagram in Figure 2.

The frequency responses and coherence measures derived from the flight data provide cues about what dynamic effects are dominant in the different parts of the frequency range as well as dynamic coupling. Good example are the angular responses (roll rate p and pitch rate q) to the cyclic inputs (lateral input δ_{lat} and longitudinal input δ_{lon}). The corresponding frequency responses, which are illustrated in Appendix 2a and 2b, show a pronounced lightly-damped second-order behavior. This characteristic is present for both the on-axis and the off-axis responses. The second-order nature of the response results from a dynamical coupling, namely the coupling between the airframe angular motion and the regressive rotor flap dynamics (blade flapping a, b). The lightly damped characteristic is due to the presence of a stabilizer bar [4].

Lateral and Longitudinal Fuselage Dynamic Equations

From the Newton-Euler equations we derive the four equations for the lateral and longitudinal linear and angular fuselage motions:

$$\dot{u} = (-w_0 q + v_0 r) - g\theta + X_u u + X_a a \tag{2}$$

$$\dot{v} = (-u_0 r + w_0 p) + g\phi + Y_v v + Y_b b \tag{3}$$

$$\dot{p} = L_u u + L_v v + L_b b \tag{4}$$

$$\dot{q} = M_u u + M_v v + M_a a \tag{5}$$

The external aerodynamic and gravitational forces and moments are formulated in terms of stability derivatives [8]. For example, the rotor forces are expressed through the rotor derivatives X_a, Y_b, and the rotor moments through the flapping spring-derivatives L_b, M_a. General aerodynamic effects are expressed by speed derivatives such as $X_u, Y_v, L_u, L_v, M_u, M_v$. The centrifugal terms in the linear-motion equations, which are function of the trim condition (u_0, v_0, w_0), are relevant only in cruise flight.

Rotor/Stabilizer-Bar Dynamics

The simplest way to represent the rotor dynamics is as a rigid disc which can tilt about the longitudinal and lateral axis. This motion corresponds to the first harmonic approximation in

the Fourier Series description of the rotor flapping equations. The resulting rotor equations of motions are two first order differential equations, for the lateral and longitudinal flapping:

$$\tau_f \dot{b} = -b - \tau_f p + B_a a + B_{lat}\delta_{lat} + B_{lon}\delta_{lon} \quad (6)$$

$$\tau_f \dot{a} = -a - \tau_f q + A_b b + A_{lat}\delta_{lat} + A_{lon}\delta_{lon} \quad (7)$$

In our initial application of system identification to the modeling of the R-50 [9], we were treating the rotor/stabilizer bar as a lumped system. The resulting model was accurate. However because the stabilizer bar has a major influence on the helicopter's flight-dynamic characteristics, we decided to explicitly model the stabilizer bar system. This will allow better study of the effects of the stabilizer bar during flight control design or handling quality evaluations.

The stabilizer bar can be regarded as a secondary rotor, attached to the rotor shaft above the main rotor, through an unrestrained teetering hinge. The blades consist of two simple paddles. The stabilizer bar receives cyclic inputs from the swash-plate in a similar way as the main blades. Because of the teetering hinge and the absence of restraint, the stabilizer bar is virtually not subject to cross axis effects (the stabilizer bar restoring forces are entirely centrifugal, resulting in a resonant frequency for the flapping motion which is identical to the rotor rotation speed. Therefore, independently of the amount of damping in the system, the phase lag between the control input and the dynamic response is exactly $90°$). We can write the lateral (d) and longitudinal (c) stabilizer bar dynamic equations using the same equations as for the single rotor system (Eq. 6-7) but in an uncoupled form:

$$\tau_s \dot{d} = -d - \tau_s p + D_{lat}\delta_{lat} \quad (8)$$

$$\tau_s \dot{c} = -c - \tau_s q + C_{lon}\delta_{lon} \quad (9)$$

Where D_{lat} and C_{lon} are the input derivatives, and τ_S is the stabilizer bar's time constant, which is a function of the paddle lock number γ_S and the rotor speed Ω.

The stabilizer bar does not exert any forces or moments on the shaft. The bar dynamics are coupled to the main rotor via the bell mixer. The bell mixer is a mechanical mixer, which superposes a cyclic command proportional to the amount of stabilizer bar flapping to the cyclic commands coming from the swash-plate. The resulting augmented lateral and longitudinal main rotor cyclic commands can be written as:

$$\bar{\delta}_{lat} = \delta_{lat} + K_d d \text{ and } \bar{\delta}_{lon} = \delta_{lon} + K_c c \quad (10)$$

The gains K_d and K_C are the stabilizer bar gearing, which are functions of the geometry of the bell mixer. Applying the Laplace transformation to the stabilizer bar lateral flapping equations (Eq. 8-9) we obtain:

$$d = \frac{-\tau_s}{\tau_s s + 1} p + \frac{D_{lat}}{\tau_s s + 1}\delta_{lat} \quad (11)$$

which shows that the stabilizer bar does indeed act as a lagged rate feedback.

Using the same tip-path plane model formulation for the single rotor flapping equations, and introducing the augmented cyclic commands gives:

$$\tau_f \dot{b} = -b - \tau_f p + B_a a + B_{lat}(\delta_{lat} + K_d d) + B_{lon}\delta_{lon} \quad (12)$$

$$\tau_f \dot{a} = -a - \tau_f q + A_b b + A_{lat}(\delta_{lat} + K_c c) + A_{lon}\delta_{lon} \quad (13)$$

where B_{lat}, B_{lon} and A_{lon}, A_{lat} are the input derivatives, τ_f is the main rotor time constant, which is a function of the main blade lock number γ and the rotor speed Ω. B_a and A_b account for the cross-coupling effects occurring at the level of the rotor itself.

In the final state-space model, the control augmentation is determined through the system's states. Therefore, we need to define the derivatives: $B_d = B_{lat} K_d$ and $A_c = A_{lon} K_c$. The relation between the derivatives and the gearing of the bell-mixer are:

$$K_d = \frac{B_d}{B_{lat}} \text{ and } K_c = \frac{A_c}{A_{lon}} \quad (14)$$

In reality, since the bell-mixer operates the same way independently of the rotor azimuth, the gearing is the same for both axes. The gearing value was determined experimentally. This relation of Eq. 14 could be used as a constraint between the derivatives B_{lat} and B_d (A_{lon} and A_c) to reduce the number of unknown parameters. However, since we were not certain about our approach to the modeling of the stabilizer bar, we decided to leave them free (we will compare the identified value to the value obtained experimentally).

Heave Dynamics

The frequency response of the vertical acceleration to collective (az/col in Appendix 2a and 2b), shows that a first order system should adequately capture the heave dynamics. This agrees with the rigid body equations from the Newton-Euler equations:

$$\dot{w} = (-v_0 p + u_0 q) + Z_w w + Z_{col} \delta_{col} \quad (15)$$

The term in parenthesis same as in Eq. 2 and 3 corresponds to the centrifugal forces that a relevant for the cruise conditions. Note that the response does not exhibit the peak in magnitude caused by the inflow effects, typical of full-size helicopters. This is because the flap frequency for the R-50 ($1/\text{rev} = 89$ rad/s) is well beyond the frequency range of identification and of piloted excitation (30 rad/s).

Yaw Dynamics

The yaw dynamics of the bare helicopter airframe can usually be modeled as the simple first order system:

$$\frac{r}{\delta_{ped}} = \frac{N_{ped}}{s - N_r} \quad (16)$$

where N_r is the bare airframe yaw damping coefficient and N_{ped} is the sensitivity to the pedal control.

However, in our case, an artificial yaw damping system was used during the flight testing and we would like to explicitly account for this dynamic augmentation.

Our yaw damping system is obtained through a yaw-rate feedback. Since, at the time of the flight experiment, only the pilot pedal input δ_{ped} and the helicopter yaw rate r were measured, ground experiments were performed to isolate the dynamics of the tail actuator and yaw rate gyro. The dynamics of the actuator and rate gyro were described by their respective frequency responses T_{act} and T_{gyro}. By expressing the yaw dynamics of the bare airframe as the frequency response $T_{r\delta}$, we can formulate the frequency response of the augmented yaw dynamics as:

$$T_{r\delta,aug} = \frac{T_{r\delta} T_{act}}{1 + T_{r\delta} T_{act} T_{gyro}} \quad (17)$$

Since $T_{r\delta,aug}$ is known from the flight experiments we can solve for the unknown bare airframe dynamics $T_{r\delta}$ using frequency response arithmetic.

$$T_{r\delta} = \frac{T_{r\delta,aug}}{T_{act} - T_{r\delta,aug} T_{act} T_{gyro}} \tag{18}$$

The resulting frequency response for the bare airframe yaw dynamics $T_{r\delta}$ did not exhibit the first order form of Eq. 16. From this we conclude that other dynamic effects, such as the engine drive-train dynamics, influence the yaw dynamics.

To avoid increasing the complexity of the model, we decided to revert to the representation we used in [9]. There, we assume that the augmented yaw dynamics could be modeled as the first order bare airframe dynamics with a yaw rate feedback represented by a simple first order low-pass filter:

$$\frac{r_{fb}}{r} = \frac{K_r}{s + K_{rfb}} \tag{19}$$

The closed loop transfer function for the augmented yaw rate response becomes:

$$\frac{r}{\delta_{ped}} = \frac{N_{ped}(s + K_{rfb})}{s^2 + (K_{rfb} - N_r)s + (K_r N_{ped} - N_r K_{rfb})} \tag{20}$$

With the corresponding differential equations used in the state-space model:

$$\dot{r} = N_r r + N_{ped}(\delta_{ped} - r_{fb}) \tag{21}$$

$$\dot{r}_{fb} = -K_{rfb} r_{fb} + K_r r \tag{22}$$

Again, since we have only the measurements of the pilot input δ_{ped} and the yaw rate r, the above representation is over-parameterized. One constraint between two parameters must be added in order to avoid having problems during the identification due to correlated parameters. As constraint, we stipulate that the pole of the low-pass filter must be twice as fast as the pole of the bare airframe yaw dynamics:

$$K_{rfb} = -2 \cdot N_r \tag{23}$$

With this constraint, a low transfer function cost is attained. However the value obtained for the bare airframe yaw damping N_r, is not necessarily physically meaningful. However, this should not constitute a big limitation since the active yaw damping system can be retained in future flight control designs as part of the bare airframe dynamics.

Offset Equations

In the speed equations (Eq. 2-3), the derivatives X_a and Y_b should theoretically be equal respectively to plus and minus the value of the gravity ($g = 32.2\,\text{ft/s}^2$). Enforcing that constraint is possible only if the flight-data has been properly corrected for the position offset in the sensor location relative to the C.G. Since, in our case, the C.G. location is not known with sufficient accuracy, we have explicitly accounted for a vertical offset h_{cg} by relating the measured speeds (v_m, u_m) to the speed at the C.G. (v, u).

$$v_m = v - h_{cg} p \tag{24}$$

$$u_m = u + h_{cg} q \tag{25}$$

Using this method, we were able to enforce the constraint $-X_a = Y_b = g$, and, at the same time, identify the unknown vertical offset h_{cg}.

Swash-Plate Actuator Dynamics

The swash-plate actuators are used to implement the main rotor collective control input as well as the cyclic control inputs for the stabilizer bar and the bare rotor. Explicitly modeling

$$\begin{bmatrix} \dot{u} \\ \dot{v} \\ \dot{p} \\ \dot{q} \\ \dot{\phi} \\ \dot{\theta} \\ \tau_f \dot{a} \\ \tau_f \dot{b} \\ \dot{w} \\ \dot{r} \\ \dot{r}_{fb} \\ \tau_s \dot{c} \\ \tau_s \dot{d} \end{bmatrix} = \left[\begin{array}{cc|cc|cc|cc|ccc|cc} X_u & 0 & 0 & 0 & 0 & -g & X_a & 0 & 0 & 0 & 0 & 0 & 0 \\ 0 & Y_v & 0 & 0 & g & 0 & 0 & Y_b & 0 & 0 & 0 & 0 & 0 \\ \hline L_u & L_v & 0 & 0 & 0 & 0 & 0 & L_b & L_w & 0 & 0 & 0 & 0 \\ M_u & M_v & 0 & 0 & 0 & 0 & M_a & 0 & M_w & 0 & 0 & 0 & 0 \\ \hline 0 & 0 & 1 & 0 & 0 & 0 & 0 & 0 & 0 & 0 & 0 & 0 & 0 \\ 0 & 0 & 0 & 1 & 0 & 0 & 0 & 0 & 0 & 0 & 0 & 0 & 0 \\ \hline 0 & 0 & 0 & -\tau_f & 0 & 0 & -1 & A_b & 0 & 0 & 0 & A_c & 0 \\ 0 & 0 & -\tau_f & 0 & 0 & 0 & B_a & -1 & 0 & 0 & 0 & 0 & B_d \\ \hline 0 & 0 & 0 & 0 & 0 & 0 & Z_a & Z_b & Z_w & Z_r & 0 & 0 & 0 \\ \hline 0 & N_v & N_p & 0 & 0 & 0 & 0 & 0 & N_w & N_r & N_{rfb} & 0 & 0 \\ 0 & 0 & 0 & 0 & 0 & 0 & 0 & 0 & 0 & K_r & K_{rfb} & 0 & 0 \\ \hline 0 & 0 & 0 & -\tau_s & 0 & 0 & 0 & 0 & 0 & 0 & 0 & -1 & 0 \\ 0 & 0 & -\tau_s & 0 & 0 & 0 & 0 & 0 & 0 & 0 & 0 & 0 & -1 \end{array}\right] \begin{bmatrix} u \\ v \\ p \\ q \\ \phi \\ \theta \\ a \\ b \\ w \\ r \\ r_{fb} \\ c \\ d \end{bmatrix} + \left[\begin{array}{cc|cc} 0 & 0 & 0 & 0 \\ 0 & 0 & Y_{ped} & 0 \\ \hline 0 & 0 & 0 & 0 \\ 0 & 0 & 0 & M_{col} \\ \hline 0 & 0 & 0 & 0 \\ 0 & 0 & 0 & 0 \\ \hline A_{lat} & A_{lon} & 0 & 0 \\ B_{lat} & B_{lon} & 0 & 0 \\ \hline 0 & 0 & 0 & Z_{col} \\ \hline 0 & 0 & N_{ped} & N_{col} \\ 0 & 0 & 0 & 0 \\ \hline 0 & C_{lon} & 0 & 0 \\ D_{lat} & 0 & 0 & 0 \end{array}\right] \begin{bmatrix} \delta_{lat} \\ \delta_{lon} \\ \delta_{ped} \\ \delta_{col} \end{bmatrix}$$

Table 2 – State-space system

the stabilizer bar exposes the fast dynamics of the bare rotor. To allow for an accurate identification of the fast bare rotor dynamics, the dynamics of the swash-plate actuators must be accounted for. The dynamics of the swash-plate actuators were identified during ground experiments. An accurate fit of their frequency responses was achieved with a first order transfer function:

$$G_R(s) = \frac{15}{s+15} \tag{26}$$

State-Space Identification

The full state-space model of the R-50 dynamics is obtained by collecting all the differential equations in a matrix differential equation:

$$M\dot{\bar{x}} = F\bar{x} + G\bar{u} \tag{27}$$

with state vector $\bar{x}$ and input vector $\bar{u}$. The system matrix F contains the stability derivatives, the input matrix G contains the input derivatives, and the M matrix contains the rotor time constants for the rotor flapping equations. The full state-space system is depicted in Table 2.

From the coherence measure obtained during the multivariable frequency domain analysis, we select the frequency responses that should be used for the state-space identification and, for each response, what frequency range should be used for the fitting. The final structure is obtained by adding and removing derivatives according to the quality of the frequency domain fit and statistical information about the derivatives. The useful statistics are the insensitivity of the cost function to each derivative and the correlation between the derivatives. Insensitive and/or correlated parameters are dropped.

A helicopter responds differently in hover flight than it does in cruise flight. We observed that, for our system, these differences did not significantly affect the model structure, but rather were mostly absorbed in the derivatives. For the cruise flight condition, because of the non-negligible speed, we had to account for the centrifugal acceleration terms which appear in the equation of motion of the fuselage's linear accelerations (Eq. 2-3). The average trim condition for the forward flight experiments is $u_0 = 49.2$ ft/s, $v_0 = -11$ ft/s, and $w_0 = 0$ ft/s. All

	Hover	Cruise		Hover	Cruise
VX /LAT	15.741	-	Q /LON	41.308	9.696
VY /LAT	18.424	-	AX /LON	27.915	48.752
VZ /LAT	-	71.105	AY /LON	35.035	-
P /LAT	61.539	12.955	AZ /LON	33.805	44.240
Q /LAT	50.376	18.468	P /COL	-	45.835
AX /LAT	15.741	-	Q /COL	-	19.143
AY /LAT	17.363	23.469	R /COL	35.217	-
R /LAT	27.382	-	AZ /COL	55.276	78.184
AZ /LAT	24.969	-	AY /PED	-	10.278
VX /LON	27.915	-	VY /PED	-	39.134
VY /LON	35.035	-	R /PED	18.841	23.542
VZ /LON	-	48.521	AZ /PED	19.406	-
P /LON	37.067	15.555	**Average**	**31.492**	**33.925**

Table 3 – Transfer Function Costs

differences are visible in Appendix 1, which shows the parameter values and associated statistics, and in s 3, which shows the costs achieved by each transfer function, and indicates which frequency responses are relevant for the two operating conditions.

6 Results and Discussion

6.1 Frequency Response Agreement

The predicted frequency responses from the identified model show a good agreement with the frequency responses from the flight-data, both in hover and cruise conditions. The transfer function costs are given in Table 3 and the frequency response comparison is depicted in Appendix 2a and 2b. Compared with the results obtained for the lumped rotor/stabilizer bar [9], the off-axis angular responses (p to δ_{lon} and q to δ_{lat}) have been significantly improved by explicitly modeling the stabilizer bar. This close agreement is better than what is usually achieved in full-size helicopters. This can be attributed to the dynamics of the model-scale helicopter being dominated by the rotor dynamics and to the absence of complex aerodynamic effects.

6.2 Identified Model Parameters

The Table in Appendix 1 gives the numerical values of the identified derivatives and their associated accuracy statistics: the Cramer-Rao percent (C.R.%) and the insensitivity (I%) of the derivatives. These statistics indicate that all of the key control and response parameters are extracted with a high degree of precision [6]. Notice that most of the quasi-steady derivatives have been dropped, thus showing that the rotor plays a dominant role in the dynamics of model-scale helicopters. This is also reflected by the number of rotor flapping derivatives $()_b$ and $()_a$. The term *actuated helicopter* is a good idealization of the dynamics of the model-scale helicopter, where the rotor dominates the response.

Rotor Parameters

For the hover condition, the identified stabilizer bar and bare rotor time constants came out as respectively $\tau_s = 0.34\,\mathrm{s}$ and $\tau_f = 0.046\,\mathrm{s}$. These values are close to the theoretical values of $\tau_s = 0.36\,\mathrm{s}$ and $\tau_f = 0.053\,\mathrm{s}$, predicted from the lock numbers γ of the respective blades and the rotor speed Ω.

$$\tau = \frac{16}{\gamma\Omega} \tag{28}$$

The blade lock number describes the ratio between the aerodynamic and inertial forces acting on the blade.

$$\gamma = \frac{\rho c_p c_\alpha (R^4 - r^4)}{I_b} \tag{29}$$

It is defined by the air density ρ, the blade chord length c_p, the lift curve slope c_α, the inside and outside radii of the blade r, R, and the blade inertia I_b.

For the main blade the effective lock number γ_{eff} was used to account for the inflow effects.

$$\gamma_{eff} = \frac{\gamma}{1 + c_\alpha \sigma / 16 \nu_0} \tag{30}$$

where σ, is the rotor solidity, and ν_0 is the inflow ratio derived from the thrust coefficient ($\nu_0 = \sqrt{0.5 c_{T_0}}$).

These results also validate our results from our earlier work, where the main rotor and stabilizer bar were modeled as a lumped system. We can now state that the time constants identified at the time (τ=0.38s) belonged in fact to the stabilizer bar. This shows that the stabilizer bar dominates the rotor response characteristics and behaves like a model following controller.

In cruise condition the rotor time constants decreases to $\tau_s = 0.26$ s and $\tau_f = 0.035$ s, which is an anticipated result.

The stabilizer bar couples to the main rotor, through the derivatives B_d and A_c. By applying Equation 14, we can calculate the equivalent bell-mixer gearing. The result of $K_d = 10.92$ and $K_c = 12.88$ for, respectively, the lateral and longitudinal axes, are close to the real gearing $K = 13.58$ determined experimentally. In forward flight, the equivalent gearing become: $K_d = 10.73$ and $K_c = 13.79$. Which agrees with the reality that the gearing is constant.

The identified roll and pitch rotor spring derivatives are respectively $L_b = 166.1$ and $M_a = 82.57$, for hover conditions. Their values for cruise condition are about 30% larger: $L_b = 213.2$ and $M_a = 108$, which is an expected effect.

The lateral and longitudinal main rotor control derivatives have reasonable values with only slight changes between hover and cruise conditions. The only exception is B_{lon}, which is 45% larger in cruise flight, indicating a higher cross axis activity. The stabilizer bar control derivatives are almost identical for both flight conditions, which validates the idea that their design is aerodynamically neutral.

These physically meaningful results indicate that the hybrid model structure with the stabilizer bar augmentation accurately captures the rotor dynamics and its coupling with the fuselage.

Quasi-Steady Derivatives

The speed derivatives X_u, Y_v, in the equations (Eq. 2-3), have the sign and relative magnitudes expected for hovering helicopters, but the absolute magnitudes are all considerably larger (2-5 times) than those for full scale aircraft. This is expected from the dynamic scaling relationships as discussed later. In cruise flight the longitudinal speed derivative X_u increases significantly. Note that this derivative has the highest insensitivity of all derivatives (29.6 and 27.5 for, respectively, hover and cruise flight), as well as a very high Cramer-Rao percent.

Therefore, the identified value is unreliable. This poor result is related to the insufficient low frequency information content of the flight data. It can be improved by longer record lengths.

The speed derivatives L_u, L_v and M_u, M_v in the angular rate equations (Eq. 4-5) contribute a destabilizing influence on the phugoid dynamics. These derivatives were dropped for the cruise conditions.

With the help of the offset equations (Eq. 24-25) we were able to constrain the force coupling derivatives to gravity ($-X_a = Y_b = g$) and, at the same time, identify the vertical C.G. offset which came out to be $h_{cg} = -0.41$ ft in hover conditions and $h_{cg} = -0.32$ ft in cruise conditions. The difference of 0.09 ft (2.7 cm) can be attributed to fuel level changes or aerodynamic drag.

Yaw Dynamics

Little can be said with regard to the yaw dynamics since the model structure poorly reflects the physical reality. We can note that the yaw damping has the correct negative sign, and that the yaw rate feedback coefficients stay virtually constant between hover and cruise conditions. The major changes are those affecting the yaw control derivative N_{ped}, which decreases, and the lateral speed derivative N_v which increases drastically in forward flight. Both results are consistent with the expectations. A time delay of was identified to account for the high-frequency un-modeled dynamics.

Heave Dynamics

The heave damping derivative Z_w has the correct sign. In cruise flight, the larger heave damping and heave control sensitivity Z_{col} is correct. The latter is directly related to the higher efficiency of the rotor in cruise flight (translational lift).

6.3 Time Domain Verification

For the time domain verification, special flight experiments using doublet-like control inputs were performed in hover and forward flight. The recorded inputs are used as inputs to the identified model, and the helicopter responses predicted by the model are compared to the responses recorded during the flight test. The results from the comparison are presented in Appendix 3a and 3b, for, respectively, the hover and cruise condition. Overall, excellent agreement is achieved both in hover and forward flight. However, two weak points are noticeable.

First is the poor agreement of the yaw response to secondary inputs. The highest mismatch is obtained for the response to the lateral cyclic input. This problem is due to the approximate way the yaw dynamics and the active yaw damping system were modeled as well as the likely omission of some aerodynamic effects.

The second weak point is the poor agreement for the speed and acceleration responses to secondary inputs in the cruise condition. This is a direct result of the improperly identified quasi-steady and speed derivatives, related to the insufficient low frequency content of the cruise flight-data.

It is important to notice that the accuracy of the identified linear model is excellent up to fairly large flight incidences and large excursions from the operating point. For example the helicopter attitudes reach values up to 40 degrees for roll and up to 20 degrees for pitch. The cruise flight model covers a speed range from 10 to 20 m/s.

Table 4a – Eigenvalues and modes for hover flight

λ#	Eigenvalue Location	Mode Description for Hover Model
1-2	0.3061± 0.094 (ζ=-0.9562; ω=0.3201)	unstable phugoid type mode involving the lateral and longitudinal velocities and the pitch and roll angles
3-4	-0.4007± 0.086 (ζ=0.9778; ω=0.4098)	stable phugoid type mode involving the lateral and longitudinal velocities and the pitch and roll angles
5	-0.6079	damped yaw-heave mode
6-7	-1.699± 8.192 (ζ=0.2031; ω=8.366)	lightly damped pitch mode with a 70% rolling component corresponding to the coupled fuselage/rotor/stabilizer bar mode
8-9	-6.196± 8.198 (ζ=0.6029; ω=10.28)	damped yaw mode (active yaw damping)
10-11	-2.662± 11.58 (ζ=0.2241; ω=11.88)	lightly damped roll mode with a 50% pitching component corresponding to the coupled fuselage/rotor/stabilizer bar mode
12-13	-20.17± 4.696 (ζ=0.9739; ω=20.71)	critically damped high frequency roll mode with a 40 % pitching component

Table 4b – Eigenvalues and modes for cruise flight

λ#	Eigenvalue Location	Mode Description for Cruise Model
1	-0.1216	damped longitudinal mode
2	-0.9614	damped yaw-heave mode
3	-1.838	damped yaw-heave mode involving the lateral velocity (tail-fin effect)
4-5	-2.321± 8.794 (ζ=0.2552; ω=9.095)	lightly damped pitch mode with a 90% rolling component corresponding to the coupled fuselage/rotor/stabilizer bar mode
6-7	-5.005± 8.133 (ζ=0.5241; ω=9.549)	damped yaw mode (active yaw damping)
8-9	-3.396± 12.43 (ζ=0.2636; ω=12.88)	lightly damped roll mode with a 10% pitching component corresponding to the coupled fuselage/rotor/stabilizer bar mode
10-11	-27.04± 7.019 (ζ=0.9679; ω=27.94)	critically damped high frequency roll mode with a 40 % pitching component

6.4 Eigenvalues and Dynamic Modes

Important dynamic characteristics of the R-50 can be understood from eigenvalues and eigenvectors computed from the identified model. Tables 4 lists the eigenvalues and the dynamic modes obtained for the hover and the cruise condition.

We can relate some of the modal characteristics to our identified derivatives. For example, for the hover conditions, the frequency of the coupled fuselage/rotor/stabilizer modes for pitch and roll can be related to the square root of the pitch flap spring ($\sqrt{M_a} = 9.1$rad/s), respectively the square root of the roll flap spring ($\sqrt{L_b} = 12.9$rad/s). Moreover, we can show that the small damping ratio of these modes directly reflects the large rotor time constant introduced by the presence of the stabilizer bar [4], for example, in the roll axis: $\zeta_{roll-flap} = 1/(2\tau_s \sqrt{L_b}) = 0.11$, and in the pitch axis: $\zeta_{pitch-flap} = 1/(2\tau_s \sqrt{M_a}) = 0.16$.

6.5 Dynamic Scaling

To determine how the flight dynamics of a miniature helicopter compare with the flight dynamics of its full-size counterpart, the key characteristics of the identified R-50 are compared to those of a full-size helicopter, dynamically scaled to the same rotor diameter. The Bell UH-1H was selected for the comparison because its design is similar to the R-50 (2 bladed teetering rotor equipped with a Bell stabilizer bar). Dynamic (or "Froude") scaling was

Table 5 – Comparison of R-50 and dynamically-scaled UH-1H characteristics, N=4.76

Parameter	UH-1H full-scale	Scaling rule	UH-1H model-scale	R-50
R, rotor radius (ft)	24	1/N	5.04	5.04
W, weight (lb)	8000	$1/N^3$	74	150
Ω, rotor speed (rad/s)	34	$\sqrt{N}$	76.1	89.01
I_b ,blade inertia,(s-ft^2)	1211	$1/N^5$	0.495	0.87
γ_b, blade Lock number	6.5	1	6.5	3.44
C_T/σ	0.0606	1	0.0606	0.0896
h_{rot}/R , rotor hub height	0.29	1	0.29	0.36
L_b, flap spring (rad/s^2)	19.2	N	96.77	166.1
$\omega_{roll\text{-}flap}$ (rad/s)	4.38	$\sqrt{N}$	9.83	11.88
$\tau_s\Omega$, non-dim. rotor flap time constant (rotor rev.)	5.7	1	5.7	4.84

applied to ensure that the model scale and full-scale vehicles shared common ratios of inertia-to-gravity and aerodynamic-to-gravity forces. The geometric and dynamic characteristics of the model scale (subscript m) and full scale aircraft (subscript a) were then related via a well known set of similarity laws [10] based on scale ratio N (e.g., N=5 refers to a 1/5–th scale model):

Length:	$L_m = L_a / N$
Time constant:	$T_m = T_a / \sqrt{N}$
Weight:	$W_m = W_a / N^3$
Moment of inertia:	$I_m = I_a / N^5$
Frequency:	$\omega_m = \omega_a \sqrt{N}$

Table 5 shows a comparison of the key configuration parameters and identified dynamic characteristics for the R-50 with the model-scale equivalents for the UH-1H. The scale ratio is N=4.76, or nearly 1/5-th scale. The R-50 is seen to be about twice as heavy as a scaled down UH-1H. This is mainly due to the high payload weight (53lbs). This results in a higher normalized thrust coefficient (C_T/σ) than would otherwise be expected. The R-50 blades are also relatively heavier, resulting in a lower Lock number than the UH-1H. These increased relative weights appear to be typical of small-scale flight vehicles as seen from reference to the scaled data for the TH-55 [11]. The higher flap spring is due to the elastomeric restraints on the R-50, and the combination of a teetering and flapping hinge. This configuration results in an effective hinge-offset of about 3%. The resulting roll/flap frequency is 20% higher than the scaled equivalent UH-1H. Finally, the non-dimensional rotor time constants are essentially identical (about 5 revs), showing the same strong effect of the stabilizer bar on both aircraft. Despite some detailed differences, the R-50 is seen to be dynamically quite similar to the UH-1H.

7 Conclusions

System identification techniques as used in full-scale helicopters have been successfully applied to model-scale unmanned helicopters. The results are better than what is usually

achieved with full-scale helicopters. This is partly due to the dominance of the rotor in the dynamics and to the absence of complex aerodynamic and structural dynamic effects.

The same frequency-sweep flight testing method as for full-scale helicopters can be applied to model-scale helicopters. The flight testing for hover flight conditions is not problematic. The forward flight condition is more challenging, but reasonable results can be obtained by using simple experimental methods.

Good results of system identification depend on a high quality instrumentation and an optimal integration of the sensor information.

CIFER® system identification techniques were effectively used to derive an accurate high-bandwidth model for the R-50 in both hover and forward flight conditions. The few weaknesses of the models — which are well understood — could be addressed, if necessary. The identified model should be well suited to flight control design, handling quality evaluation, and simulation applications.

The R-50 was shown to be dynamically quite similar to the scaled UH-1H, that is, the dynamics of miniature helicopter follow simple scaling rules. The R-50 is proportionally heavier (aircraft weight and blade inertia) and has a small effective hinge-offset (3%) due to the elastomeric restraints and the teetering/flapping hinge combination. The dynamics of both helicopters are strongly influenced by the stabilizer bar.

References

[1.] Zhu, X. and M. Van Nieuwstadt, "The Caltech Helicopter Control Experiment." 1996, California Institute of Technology, CDS Technical Report 96-009.

[2.] Bruce, P.B., J.E.F. Silva, and M.G. Kellett. "Maximum Likelihood Identification of a Rotary-Wing RPV Simulation Model From Flight-Test Data." in *AIAA Atmospheric Flight Mechanics Conference and Exhibit*. 1998. Boston, Massachusetts.

[3.] Tischler, M.B. and M.G. Cauffman, "Frequency-Response Method for Rotorcraft System Identification: Flight Application to BO-105 Coupled Rotor/Fuselage Dynamics." *Journal of the American Helicopter Society*, 1992. 37/3: p. 3-17.

[4.] Heffley, R.K., "A Compilation and Analysis of Helicopter Handling Qualities Data; Volume I: Data Compilation." 1979, NASA.

[5.] Tischler, M.B., "System Identification Methods for Aircraft Flight Control Development and Validation." *Advances in Aircraft Flight Control*, ed. M.B. Tischler. 1995, Taylor & Francis Inc.: Bristol, PA. 35-69.

[6.] Ham, J.A., C.K. Gardner, and M.B. Tischler, "Flight-Testing and Frequency-Domain Analysis for Rotorcraft Handling Qualities." *Journal of the American Helicopter Society*, 1995(April 1995).

[7.] Hansen, "Toward a Better Understanding of Helicopter Stability Derivatives." *Journal of the American Helicopter Society*, 1982. 29-1.

[8.] Prouty, R.W., "Helicopter Performance, Stability and Control." ed. K.P. Company. 1995, Malabar, Fl: Krieger Publishing Company.

[9.] Mettler, B.F., M.B. Tischler, and T. Kanade. "System Identification of Small-Size Unmanned Helicopter Dynamics." in *55th Forum of the American Helicopter Society*. 1999. Montreal, Canada.

[10.] Burk, S.M. and C.F.W. Jr. "Radio-Controlled Model Design And Testing Techniques for Stall/Spin Evaluation of General-Aviation Aircraft." in *National Business Aircraft Meeting*. 1975.

[11.] Heffley, R.K., "Study of Helicopter Roll Control Effectiveness Criteria." 1986, NASA.

Appendix

A1. Table of Identified Parameters

A2. Frequency Responses

A3. Time Domain Verification

A1. Table of Identified Parameters

	Hover Flight			Cruise Flight			
	Value	**CR %**	**Insens. %**	**Value**	**CR %**	**Insens. %**	
M-Matrix							
τf	**0.04631**	10.87	1.64	**0.03463**	31.7	2.370	0.75
hcg	**-0.4109**	6.249	1.775	**-0.3212**	14.7	6.695	0.78
τs	**0.3415**	7.346	0.8280	**0.2591**	6.52	0.7860	0.76
F-Matrix							
Xu	**-0.05046**	62.25	29.60	**-0.1217**	57.7	27.45	2.41
Xθ, Xa	**-32.20**	constrained to *-g*		**-32.20**	constrained to *-g*		
Xr				**-11**	centrifugal term, constrained to v0		
Yv	**-0.1539**	22.92	10.90	**-0.1551**	32.66	6.844	1
Yϕ, Yb	**32.20**	constrained to *-g*		**32.20**	constrained to *-g*		
Yr				**-49.2**	centrifugal term, constrained to -u0		
Lu	**-0.1437**	12.30	3.071	-	-	-	-
Lv	**0.1432**	19.49	6.541	-	-	-	-
Lw	-	-	-	**-0.2131**	15.3	3.963	-
Lb	**166.1**	1.865	0.5996	**213.2**	0.00145	2.144	1.28
Mu	**-0.05611**	20.19	5.626	-	-	-	-
Mv	**-0.05850**	14.49	4.230	-	-	-	-
Mw	-	-	-	**0.07284**	21.2	5.676	-
Ma	**82.57**	6.283	0.5918	**108.0**	0.0593	0.7864	1..31
Ba	**0.3681**	10.48	1.125	**0.4194**	11.5	2.182	1.14
Bd	**0.7103**	4.110	0.7824	**0.6638**	9.66	1.551	0.93
Ab	**-0.1892**	11.67	4.469	**-0.1761**	21.9	9.386	0.93
Ac	**0.6439**	9.486	0.8188	**0.5773**	7.73	1.092	0.89
Zb	**-131.2**	2.765	1.619	-	-	-	-
Za	**-9.748**	19.86	8.256	-	-	-	-
Zw	**-0.6141**	10.50	4.465	**-1.011**	4.72	2.065	1.65
Zr	**0.9303**	8.151	2.754	-	-	-	-
Zp				**11**	centrifugal term constrained to -v0		
Zq				**49.2**	centrifugal term constrained to u0		
Np	**-3.525**	14.22	3.664	-	-	-	-
Nv	**0.03013**	32.51	9.082	**0.4013**	8.80	3.362	13.32
Nw	**0.08568**	14.14	5.091	-	-	-	-
Nr	**-4.129**	9.708	2.785	**-3.897**	10.57	3.673	0.94
Nrfb	**-33.07**	Nrfb=-Nped		**-26.43**	Nrfb=-Nped		0.8
Kr	**2.163**	4.417	1.736	**2.181**	7.747	2.695	1
Krfb	**-8.258**	Krfb=2Nr		**-7.794**	Krfb=2Nr		0.94
G-Matrix							
Blat	**0.1398**	7.060	1.612	**0.1237**	16.3	2.637	0.88
Blon	**0.01380**	13.35	4.214	**0.02003**	17.8	6.696	1.45
Alat	**0.03127**	7.886	2.064	**0.02654**	8.19	2.544	0.85
Alon	**-0.1004**	9.205	1.175	**-0.08372**	13.9	1.868	0.83
Zcol	**-45.84**	4.315	1.839	**-60.27**	4.06	1.862	1.31
Mcol	-	-	-	**6.980**	6.00	1.426	-
Ncol	**-3.329**	10.63	3.667	-	-	-	-
Nped	**33.07**	5.453	1.916	**26.43**	7.177	2.437	0.8
Dlat	**0.2731**	12.24	1.858	**0.2899**	12.5	2.358	1.06
Clon	**-0.2587**	10.73	1.622	**-0.2250**	11.2	1.663	0.87
Yped	-	-	-	**11.23**	21.92	4.659	-
τped	**0.09910**	13.21	6.086	**0.05893**	21.75	6.928	0.59

A2a. Frequency Responses for Hover Flight

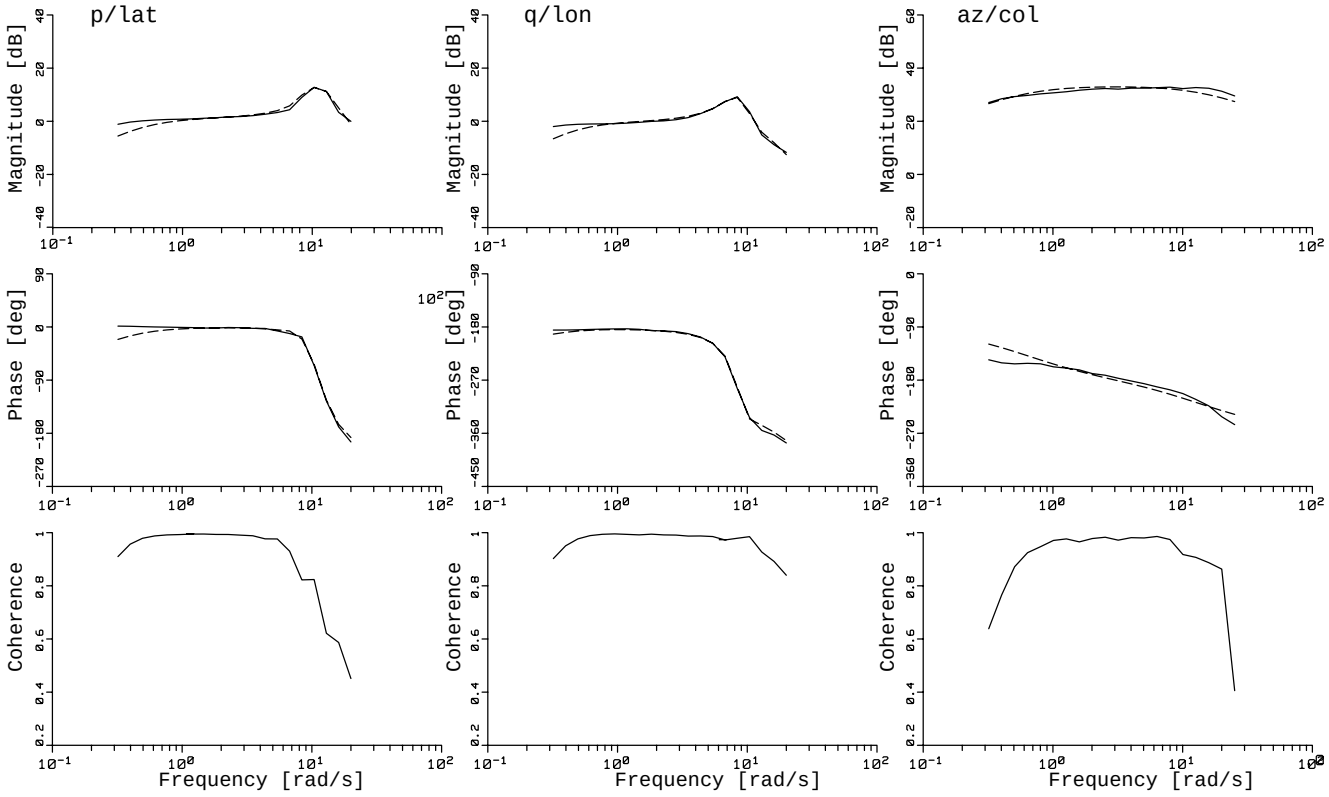

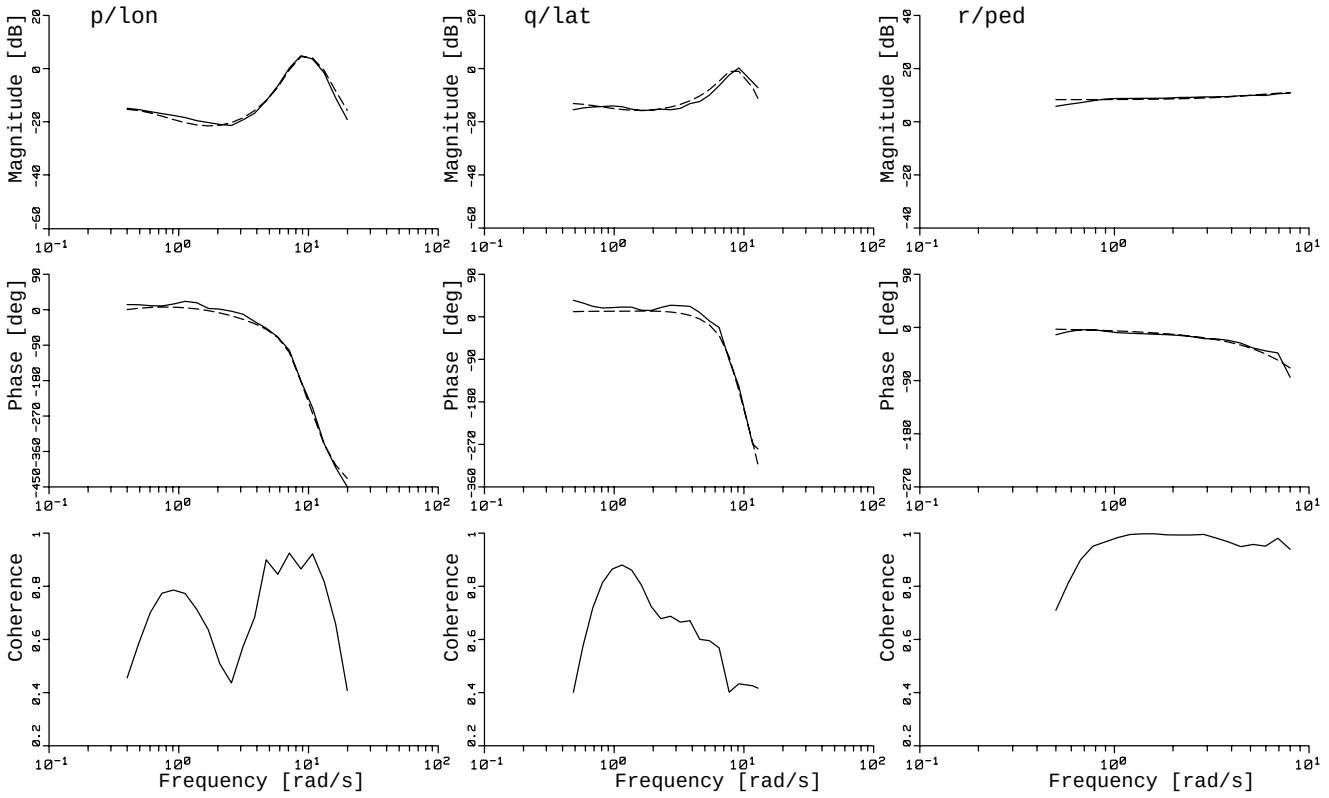

Comparison between the frequency responses computed from the identified hover model (dashed) and the frequency responses derived from the hover flight-data (solid).

A2b. Frequency Responses for Cruise Flight

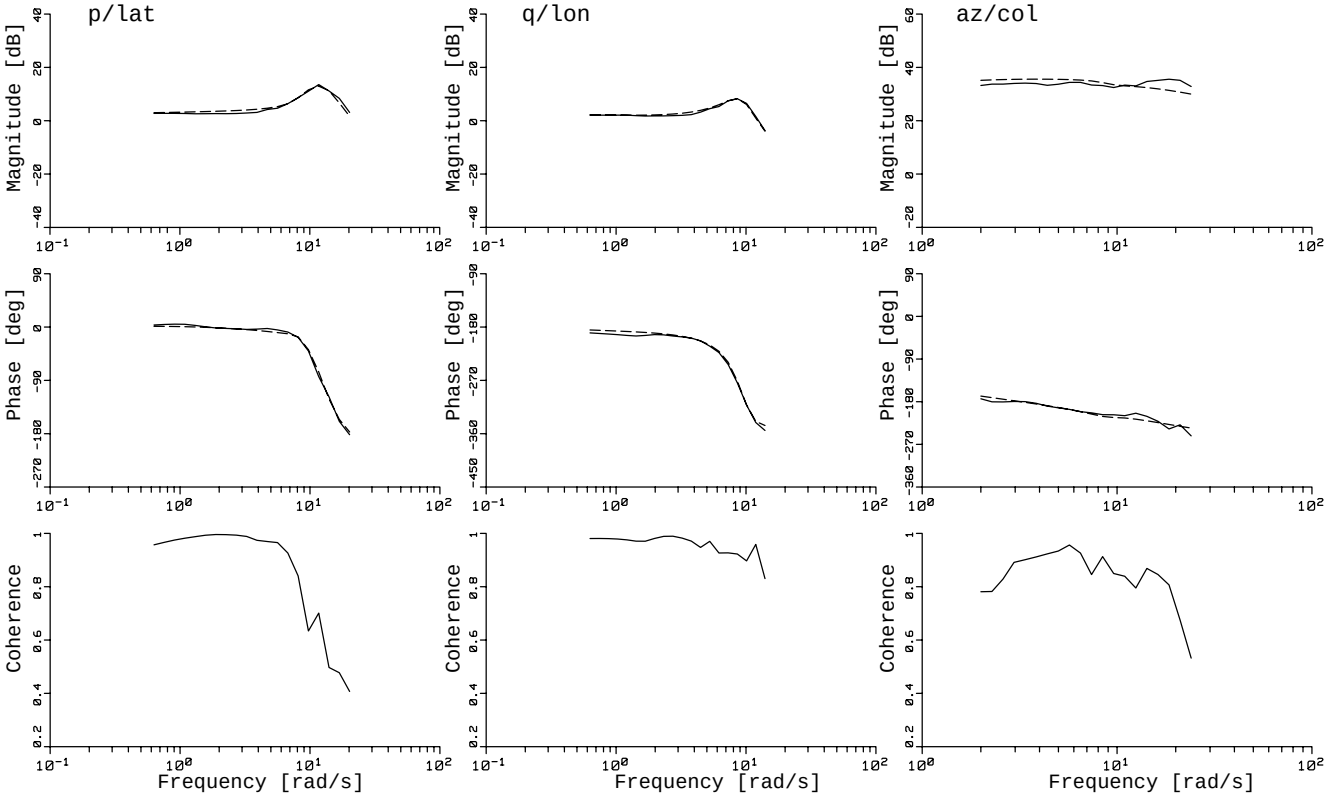

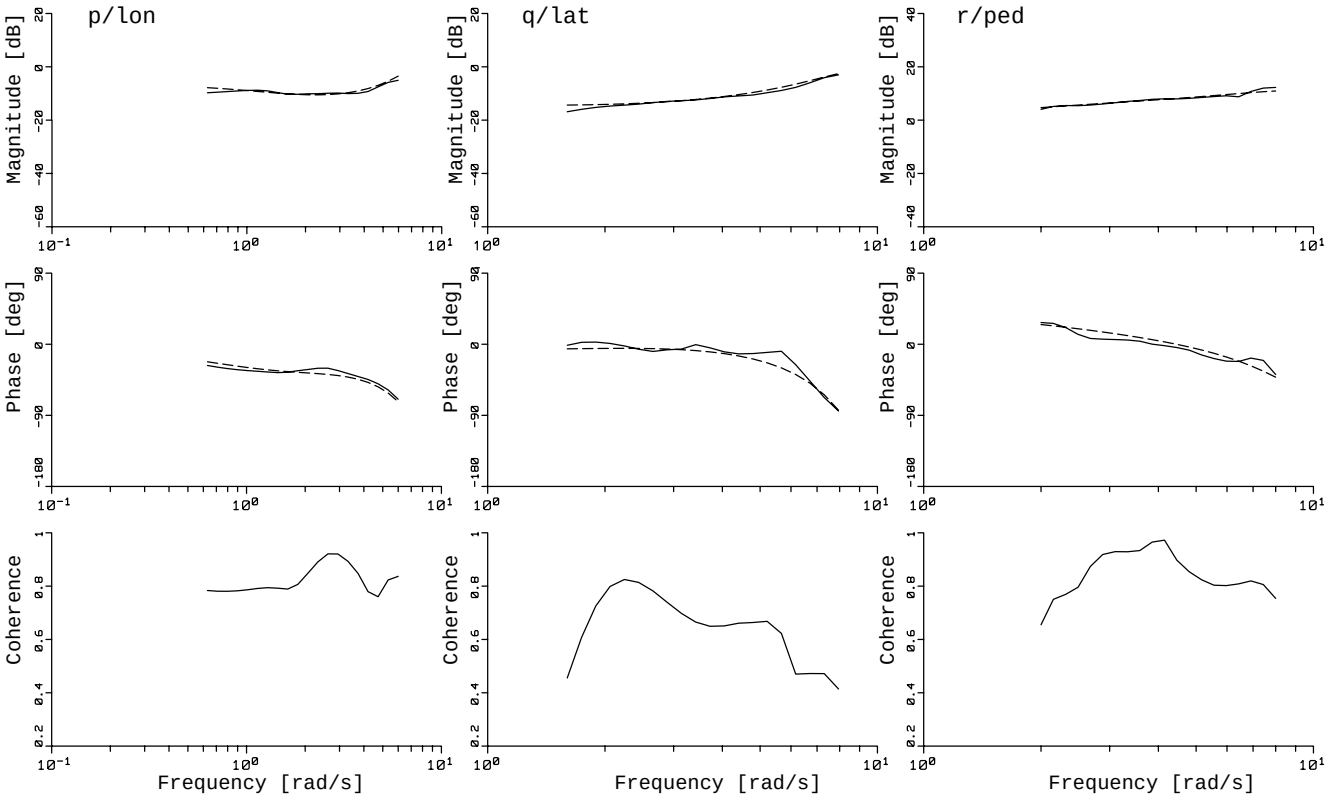

Comparison between the frequency responses computed from the identified cruise model (dashed) and the frequency responses derived from the cruise flight-data (solid).

A3a. Time Domain Verification for Hover Flight

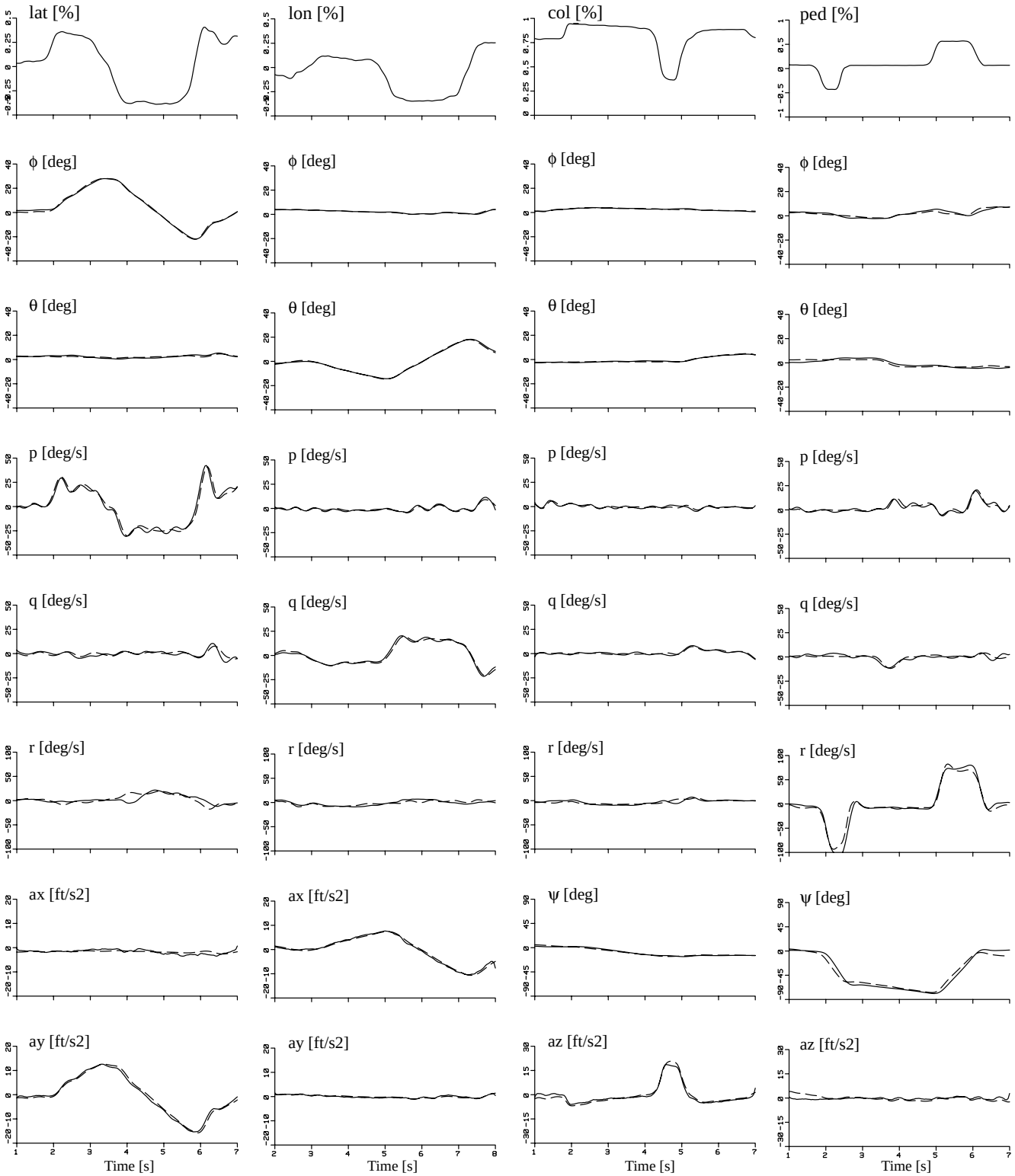

Comparison between the responses predicted by the identified hover model (dashed) and the responses obtained during flight testing in hover condition (solid).

A3b. Time Domain Verification for Cruise Flight

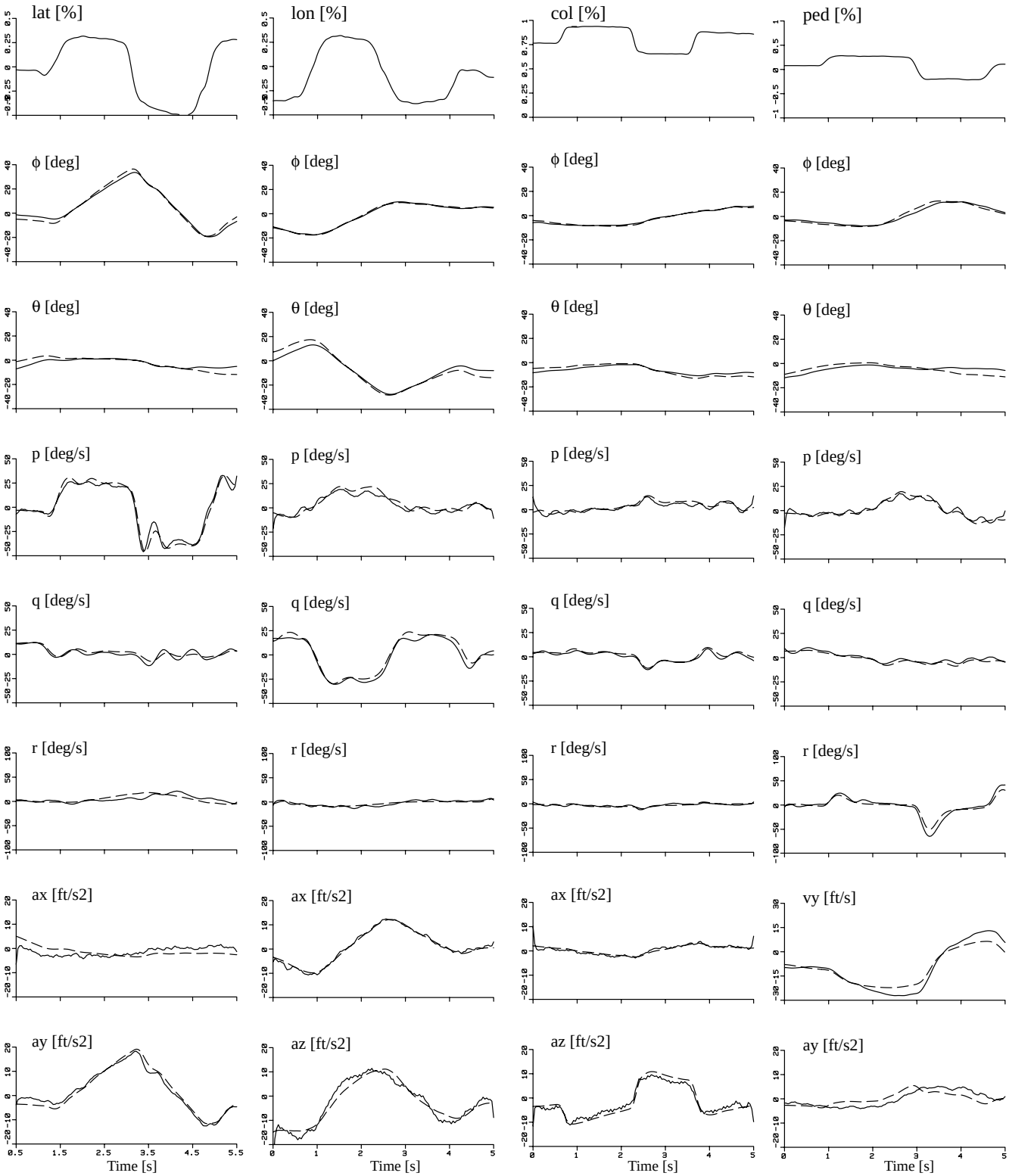

Comparison between the responses predicted by the identified cruise model (dashed) and the responses obtained during flight testing in cruise condition (solid).